Dual-sensitized modification engineering with enhanced photocatalytic degradation for organic dye

Yingying Zhao
Jilin University
Jiejing Zhang
Jilin University
Wuyou Fu (fuwy@jlu.edu.cn)
Jilin University https://orcid.org/0000-0003-3397-7427

Research Article

Keywords: photocatalytic degradation, PbS/CdS/TiO2NSs, Optical materials and properties, Heterojunction photocatalyst

Posted Date: February 26th, 2021

DOI: https://doi.org/10.21203/rs.3.rs-246705/v1

Abstract

In order to use solar irradiation efficiently, we should fabricate a high reactive photocatalyst under the visible light. It has been clearly revealed that if the titanium dioxide (TiO2) is irradiated with light, as a stable catalyst, excited electron–hole pairs of it could apply in degrading organic pollutants, but the wavelength of optical absorption is narrower than 380 nanometers. In this work, we designed and fabricated a unique TiO2 base heterojunction photocatalyst dual-sensitized by cadmium sulfide (CdS) and lead sulfide (PbS) with wide-spectrum (300-800 nm) response. Moreover, the degradation efficiency of nanocomposites reached 99.9% under visible light, which was 5 times over pure TiO2. This ternary Z-scheme structure materials will be well-promising photocatalysts.

Introduction

With the demand of development in science and technology, storage of fossil energy is nearly exhausted, simultaneously, numerous organic toxins are produced and released into water through the process of industrialization(*1-3*). Therefore, the strategy of seeking clean energy and degradation of organic pollutants has recently been the most widely investigated by multitudinous scientists(*4-6*). Nowadays, semiconductor materials have been considered in more consideration due to their attractive applications including energy conversion, storage, solar fuel, photocatalytic and medical(*7, 8*). They are regarded as potential catalyst for wastewater management and water splitting, which can directly decompose the pollutants absorbed on the surface through redox processes(*9, 10*).

TiO_2 is thought to be a suitable photocatalyst. Although, it has played an important role in stability, cost effectiveness and inert nature, they are still encountering the problems of large band gap (~3.2 eV), high recombination rate of photogenerated electron-hole pairs and narrow light response range(*11-15*). Numerous researchers have studied that combining the photoprocess with physical or chemical methods was an effective way to improve the efficiency of photodecomposition over TiO_2(*16-19*). Among them, it is one of the most effective way that building multiple heterojunction between semiconductors(*7, 20-22*).

As an important visible light-sensitive semiconductor, cadmium sulfide nanocrystal (CdS NCs) is the most investigated among the metal chalcogenides due to its direct band energy of 2.42 eV(*23-25*). Therefore, CdS is easy enough for photoexcitation of electrons and used light to a larger extent(*26*). Moreover, lead sulfide nanocrystal (PbS NCs) can be excited with less light, due to its band gap is only as narrow as 0.4 eV(*27-30*). And it is not difficult to find that its light absorption edge is in the near infrared region(*31*). As far as we know, there were only a few studies that CdS/PbS co-sensitized vertically aligned TiO_2NSs array films for photocatalytic degradation. Hence, the study of CdS/PbS/TiO_2 NSs nanocomposites is of remarkable interest and challenging.

In our work, we study a kind of unique recyclable heterogeneous PbS/CdS/TiO_2 NSs sheet nanocomposite photocatalyst. CdS and PbS play three roles in photocatalyst: (1) PbS/CdS can affect the energy band structure for nanocomposite; (2) the increasing number of quantum dots increases the specific surface area of the material; (3) building multiple heterojunction between semiconductors. Simultaneously, it may lead to a new alternative or potential technology for future photocatalyst design and improvement in practical applications.

Experimental Section

2.1 Materials

The materials for TiO_2NSs, including $Ti(OC_4H_9)_4$ and $(NH_4)_2TiF_6$ were obtained from the Tianjin Institute of Guangfu Fine Chemicals and Aladdin Reagents Co., Ltd. The materials for CdS NCs, such as $Cd(NO_3)_2{\cdot}4H_2O$, KOH, NH_4NO_3 and CH_4N_2S were purchased from Aladdin Reagents Co., Ltd. $Pb(CH3COO)_2$ and Na_2S were employed for synthesis of PbS NCs, which were obtained from Tianjin Institute of Guangfu Fine Chemicals and Xilong Chemical Co., Ltd.

2.2 Synthesis

2.2.1 TiO_2NSs

$Ti(OC_4H_9)_4$ (1 ml) and $(NH_4)_2TiF_6$ (0.5 g) were added into a solution, including deionized water (30 ml) and hydrochloric acid (30 ml). Then, the precursor solution was transferred into hydrothermal reactor (100ml) with FTO substrates, reacted for 12h at 170 ℃. Finally, the obtained product was washed with deionized water several times and dried in the air.

2.2.2 CdS NCs

The CdS NCs were synthesized by the method of chemical bath deposition (CBD). Firstly, $Cd(NO_3)_2{\cdot}4H_2O$ (0.12 g), KOH (0.5611 g), NH_4NO_3 (2.412 g) and CH_4N_2S (0.30448 g) were added into deionized water (80ml). Then, the TiO_2NSs were put into beakers with mixed solutions. Finally, the beakers were transferred into thermostat water bath, reacted 80 ℃ for 10-40min, respectively. The obtained products were abbreviated as CdS(10-40)/T.

2.2.3 PbS NCs

The PbS NCs were synthesized by successive ionic layer adsorption and reaction (SILAR) method, which were assembled onto CdS(10-40)/T. The detailed synthetic process are as follows: Firstly, the CdS(10-40)/T were put into 0.02M $Pb(CH3COO)_2$ ethanol solution(100ml) and kept for 5min. The CdS(10-40)/T were cleaned by methanol and dried several minutes. Then, the obtained products were put into 0.02M anhydrous Na_2S methanol solution (100ml) and kept for 5min. After that, the final products were cleaned

by methanol and dried several minutes. The process of fabrication was regarded as one cycle. Meanwhile, the final products were abbreviated as PbS(nC)/CdS(10-40)/T.

2.3Characterization

All samples were tested in air condition. The measurements of X-ray diffraction were performed on Rigaku D/max-2500 diffratometer (λ=0.154056nm) with the scanning rate of 0.3° s^{-1} in the 2θ range from 20° to 80°. UV-vis curves were obtained by an UV-3150 with double-beam spectrophotometer. The samples of morphology, size and crystallographic directions images were obtained by SEM (FEI MAGELLAN 400 Scanning Electron Microscope) and the transmission electron microscope (TEM, JEM–2100F, 200 kV). The element composition and distribution were measured by EDS. The X-ray photoelectron spectra (XPS) and valence-band X-ray photoelectron spectra (VB-XPS) were obtained by the ESCALAB-250 photoelectron spectrometer. Steady-state photoluminescence (PL) spectrum was recorded on a Ramascope System (Renishaw, London, UK) with an excitation laser at wavelength of 473 nm. The light excitation current curve of the samples was obtained by a three-electrode test system. Electrochemical impedance spectroscopy (EIS) was tested by SI 1296 electrochemical interface & SI 1260 interface /grain phase analyzer.

2.4 Photocatalytic test

The test of photocatalytic activity was performed on a self-built photocatalytic reaction system, a mid-pressure Hg lamp (300 W) and a xenon lamp (XLS-150A) were selected as the light source. The catalysis (size: 3 cm1.5 cm) was added into the dye solution (700 ml, M) and stirred at 25 ℃ under UV-vis light. The method was used to evaluate the degradation efficiency of organic pollutants. Before irradiation, the suspension was stirred in the dark to reach the adsorption-desorption equilibrium on the surface of the photocatalyst. The samples (5-8ml) were selected at the same time interval, according to the photocatalytic degradation of organic pollutants. The absorption peaks, which included different concentration of the RhB or MB solution, were determined by a UV-vis spectrophotometer. The photocatalytic degradation efficiency was calculated by the formula **see formula 1 in the supplementary files.**

Results And Discussion

Figure1 shows the fabrication process of TiO_2 NSs, CdS/TiO_2 NSs and PbS/CdS/TiO_2 NSs. X-ray diffraction (XRD) measurement for TiO_2 NSs, CdS/TiO_2 NSs and PbS/CdS/TiO_2 NSs were performed as shown in Figure2a, which showed diffraction peaks at 25.34°, 37.83°, 48.10° and 55.06° corresponding to the (101), (004), (200) and (211) crystal planes of anatase TiO_2 phase (JCPDS#21-1272)(*32, 33*). Meanwhile, the blue curve presents new diffraction peaks at 43.97° and 52.08°, assigning to the (220) and (311) planes of cubic phase CdS NCs. Beyond that, the new diffraction peaks appear at 30.13° and 68.88° in green curve, assigning confirmed to (111) and (200) crystal planes of PbS NCs (JCPDS#65-2935). TEM, HTEM and SAED patterns (FigureS1) further confirmed that the samples were synthesized,

successfully. The x-ray photoelectron spectroscopy (XPS) spectrum of PbS/CdS/TiO_2NSs is shown in Figure2b. FigureS2 present the characteristic peaks position of Ti2p, Cd3d, Pb4f and S2p. The peak positions of Ti $2p_{3/2}$ and Ti $2p_{1/2}$ are located at 458.3 and 464.0 eV(*34*). The peaks of Cd $3d_{5/2}$ and Cd $3d_{3/2}$ are 405.0 and 411.7 eV, respectively. In the meantime, the peaks of S2p locate at 161.2 eV(*35*). The Pb4f is observed in FigureS2d, which is at about 138.3 eV as revealed in the previous literature(*36*). Therefore, the above results are confirmed that the preparation of the three-way PbS/CdS/TiO_2NSs catalyst is successful.

The morphology images of samples were conducted by FESEM (Figure3). Figure 3a-3b show the morphology of bare TiO_2NSs, inset picture is the cross-section of bare TiO_2NSs. It can be seen that the dense and uniform TiO_2NSs grow on the FTO substrate, vertically. The length and the thickness of TiO_2NSs are about 1.5-2.1 μm and 200-240 nm, respectively. Figure3c-3f show the images of CdS/TiO_2NSs composites with more active sites. The increase of CdS NCs is growing with the longer chemical bath deposition time (10-40 min). The more CdS NCs are growing, the more roughness of CdS/TiO_2NSs composites is improving. Figure3h-3j present the morphology of PbS/ CdS/TiO_2NSs with different cycles. The number of PbS NCs is growing with the increase in experimental cycles. The more PbS NCs are growing, the specific surface of PbS/CdS/TiO_2NSs is increasing. Therefore, a larger specific surface area is beneficial for photocatalysts. The EDS and EDS mapping spectrum of PbS/CdS/TiO_2NSs are shown in FigureS4-5. The elements of Pb, Cd and S are homogenously distributed on the TiO_2NSs surface. The atomic ratio of each element is consistent with expectations.

Figure4a illustrates the UV–vis absorption spectra of TiO_2NSs and CdS(10-40 min)/T. Meanwhile, Figure4c shows the UV–vis absorption spectra of PbS(3-5 C)/CdS(10-40 min)/T. Pure TiO_2NSs exhibited visible light absorption with absorption band edges at 380 nm. In Figure4c, the absorption edge of PbS(7C)/ CdS(40 min)/ TiO_2NSs is widened to 800 nm(*32, 36*). As shown in Figure4b and Figure4d, the UV–vis absorption spectra of PbS(3-5 C)/CdS(10-40 min)/T are red shifted as the band gap (Eg) gets narrow. Eg was computed as stated by Kubelka–Munk function (a), where c is proportionally constant, α and v are the absorption coefficient and the frequency, respectively. **See formula 2 in the supplementary files.**

The EIS measurement and steady-state photoluminescence (PL) were conducted to explore the charge transfer dynamics. Figure5a shows the EIS curves of TiO_2NSs, CdS(30)/T and PbS(5C)/CdS(30)/T. The TiO_2 NSs could exhibit higher carrier resistance than PbS(5C)/CdS(30)/T. It demonstrates that PbS(5C)/CdS(30)/T has lower electron transport resistance. Therefore, PbS(5C)/CdS(30)/T is beneficial to electrons and holes transportation. The separation of electron-hole pairs plays a key role in the photocatalytic activity of the catalyst(*37, 38*). To further explore the charge recombination dynamics, the steady-state photoluminescence (PL) was performed and the PL intensity of PbS(5C)/CdS(30)/T demonstrates an obvious decrease compared with TiO_2 NSs (Figure5b). It can be seen that the PL is quenched to some extent after the introduction of PbS and CdS. The PL quenching effect of

PbS(5C)/CdS(30)/T indicates that electrons and holes can separate, effectively. It is consistent with the EIS results (Figure5a). The transient photocurrent response is shown in Figure5c. The photoelectrochemical performance of samples has been tested for analyzing the number of photogenerated electron-hole pairs. A higher current density was achieved by PbS(7C)/CdS(30)/T than the other samples, implying the enhanced electron-hole pairs generation. Moreover, the reason of much more electron-hole pairs is due to the proper energy band matching between PbS, CdS and TiO_2. In particular, the transmitting procedure of electrons and holes is obviously shown in Figure5d.

The photocatalytic performances of the samples over RhB and MB were studied under UV-vis light. The details of reaction experiments were shown in Supplementary FigureS6. FigureS6a and FigureS6b show the UV-Vis absorption of RhB and MB dye solution degraded by the sample (30-CdS/TiO_2NSs). As shown in FigureS6c, the concentration of the organic solution did not change significantly during the dark treatment (-30-0 min). It illustrates the catalyst has no catalytic effect without driven force of solar power. Outstandingly, the degradation rate of 30-CdS/TiO_2NSs for RhB was 99.8 % within 40 min. The degradation rate of pure TiO_2 for RhB was only 23.3 % under the UV light. It is due to the smaller number of light-excited oxidative holes and the higher electron hole combination rate of bare TiO_2NSs. Meanwhile, FigureS6d shows a degradation pattern for MB analogous to that of FigureS6c, it is obvious that all of the composites sensitized with CdS quantum dots show better photocatalytic activity.

We made a comparison experiment under visible light by using a xenon lamp simulator. Clearly, according to the analysis in Figure7a, the appropriate addition of PbS QDS could enhance the catalytic property. After 160 min, 97.1 % of RhB could be removed by PbS(5C)/CdS(30)/TiO_2. The other samples, for example PbS(7C)/CdS(30)/TiO_2, show lower photocatalytic activity, it maybe owing to the increasing number of defects, recombination center and smaller surface area. Acting as recombination center of photoelectrons and holes, the defect has a negative effect on catalysis. In conclusion, CdS and PbS could effectively help TiO_2NSs to broad the light utilization range. Establishing heterogeneous nodes could accelerate the photocatalysis process. Interestingly, as confirmed by Figure5a, the electrochemical impedance spectroscopy (EIS) analysis could also agree with this.

Those response energy about photocatalytic degradation from RhB by samples sort of impetuses were greatly fitted with pseudo-first-order energy module: $-\ln(C_0/C_t)=Kt$, where C_0 is the concentration at the initial, C_t is the concentration at the reaction time t, and K is the rate constant. As shown in Figure7b, PbS(5C)/ CdS(30)/TiO_2 has a maximum K value that is much higher than the other samples. It demonstrates that the multiple heterostructure photocatalyst has high-efficiency photocatalytic activity.

In fact, the excellent recycling property and stability of photocatalysts can effectively cut the waste water treatment cost and avert secondary pollution. The stability of PbS(5C)/CdS(30)/TiO_2NSs was conducted by 5 recycling experiments in Figure7a. Specifically, there was a little drop in degradation ability after five cycles, PbS(5C)/CdS(30)/TiO_2NSs composites could still degrade 86.64% RhB. As the outermost layer of the sample, lead sulfide avoided direct light exposure to cadmium sulfide to reduce the photo-corrosion of

cadmium sulfide and improve the stability of the sample. In order to investigate the sample changes before and after the reaction, X-ray diffraction patterns were analyzed on the samples after the photocatalytic reaction. According to Figure7b, the diffraction peak of the photocatalyst has almost no change, and the sample maintains its original composition. As we expected, this result indicates that the sample exhibits excellent long-term stability. It is hopeful to achieve large-scale use without any additional pollution in the future.

The mechanism of photodegradation of dye over the catalyst is shown in Figure8. PbS is excited to produce photoelectrons under visible light irradiation. The electrons on the PbS (CB) jump to the CB of CdS and continue to transfer to TiO_2 (CB), which follows the law of conservation of energy. Meanwhile, h+ on the surface of TiO_2 (VB) should transfer to VB of CdS. Holes don't rest on CdS (VB) and jump to the valence band of PbS. The isolated electrons and h+ react with water to produce large quantities of highly oxidizing $\cdot O_2^-$ and ·OH for degradating organic pollutants.

$PbS+UV\ light \rightarrow PbS(e^-)+PbS(h^+)$ (1)

$CdS+PbS(e^-) \rightarrow CdS(e^-)+CdS(h^+)$ (2)

$CdS(e^-)+TiO_2 \rightarrow TiO_2(e^-)$ (3)

$TiO_2(e^-)+O_2 \rightarrow TiO_2+O^{2-}$ (4)

$O^{2-}+TiO_2(e^-)+H^+ \rightarrow H_2O_2$ (5)

$H_2O_2+O^{2-} \rightarrow \cdot OH+OH^-+O_2$ (6)

$OH+RhB/MB \rightarrow degraded\ or\ mineralized products$ (7)

$CdS(h^+)+RhB/MB \rightarrow degraded\ or\ mineralized\ products$ (8)

$PbS(h^+)+RhB/MB \rightarrow degraded\ or\ mineralized\ products$ (9)

As discussed, the degradation reactions can be described as the above equations (1-9).

Conclusion

In conclusion, a novel ternary PbS/CdS/TiO_2NSs heterojunction photocatalyst was successfully prepared by one-step hydrothermal method, chemical bath deposition (CBD) and successive ionic layer adsorption and reaction (SILAR). Thus, a degradation mechanism featuring heterojunction as the bridge between the photogenerated electrons and holes was proposed, which could degrade 99.9% RhB and MB solution. Transient photocurrent response indexes that the ternary PbS/CdS/TiO_2NSs composites demonstrate the ability to efficiently separate photo-generated electrons and holes and make photocatalytic activity

improved nearly 5 times. Absorption spectra experiment indicates that the absorption edge of samples has extended from 375 nm to 800 nm, the light utilization rate increased significantly. We believe that the novel three-way PbS/CdS/TiO_2NSs catalyst could have great potential in the field of energy and environmental protection. This work could provide a dual-sensitized modification engineering to construct ternary catalysts improving the degradation efficiency.

Declarations

Conflicts of interest

There are no conflicts to declare.

Acknowledgements

We are particularly grateful to the National Natural Science Foundation of China (Grant No. 51272086).

References

1. S. Mozia (2010) Photocatalytic membrane reactors (PMRs) in water and wastewater treatment. A review. *Separation and Purification Technology***73**, 71-91.
2. M. Vakili *et al.* (2014) Application of chitosan and its derivatives as adsorbents for dye removal from water and wastewater: a review. *Carbohydr Polym***113**, 115-130.
3. P. Shandilya *et al.* (2018) Fabrication of fluorine doped graphene and SmVO4 based dispersed and adsorptive photocatalyst for abatement of phenolic compounds from water and bacterial disinfection. *Journal of Cleaner Production***203**, 386-399.
4. R. Asahi, T. Morikawa, T. Ohwaki, K. Aoki, Y. Taga (2001) Visible-light photocatalysis in nitrogen-doped titanium oxides. *Science***293**, 269-271.
5. X. Liu *et al.* (2017) Noble metal-metal oxide nanohybrids with tailored nanostructures for efficient solar energy conversion, photocatalysis and environmental remediation. *Energy & Environmental Science***10**, 402-434.
6. H. Tong *et al.* (2012) Nano-photocatalytic Materials: Possibilities and Challenges. *Advanced Materials***24**, 229-251.
7. H. Wang *et al.* (2014) Semiconductor heterojunction photocatalysts: design, construction, and photocatalytic performances. *Chemical Society Reviews***43**, 5234-5244.
8. L. Jing *et al.* (2006) Review of photoluminescence performance of nano-sized semiconductor materials and its relationships with photocatalytic activity. *Solar Energy Materials and Solar Cells***90**, 1773-1787.

9. C. Chen, W. Ma, J. Zhao (2010) Semiconductor-mediated photodegradation of pollutants under visible-light irradiation. *Chemical Society Reviews***39**, 4206-4219.
10. J. Low, J. Yu, M. Jaroniec, S. Wageh, A. A. Al-Ghamdi (2017) Heterojunction Photocatalysts. *Advanced Materials***29**.
11. M. Pelaez *et al.* (2012) A review on the visible light active titanium dioxide photocatalysts for environmental applications. *Applied Catalysis B-Environmental***125**, 331-349.
12. X. Chen, L. Liu, P. Y. Yu, S. S. Mao (2011) Increasing Solar Absorption for Photocatalysis with Black Hydrogenated Titanium Dioxide Nanocrystals. *Science***331**, 746-750.
13. A. Fujishima, X. Zhang, D. A. Tryk (2008) TiO2 photocatalysis and related surface phenomena. *Surface Science Reports***63**, 515-582.
14. G. Williams, B. Seger, P. V. Kamat (2008) TiO2-graphene nanocomposites. UV-assisted photocatalytic reduction of graphene oxide. *Acs Nano***2**, 1487-1491.
15. X. Li *et al.*, (2008) Preparation of polyaniline-modified TiO2 nanoparticles and their photocatalytic activity under visible light illumination. *Applied Catalysis B: Environmental***81**, 267-273.
16. M. Sathish, B. Viswanathan, R. P. Viswanath, C. S. (2005) Gopinath, Synthesis, characterization, electronic structure, and photocatalytic activity of nitrogen-doped TiO2 nanocatalyst. *Chemistry of Materials***17**, 6349-6353.
17. U. G. Akpan, B. H. Hameed (2010) The advancements in sol-gel method of doped-TiO2 photocatalysts. *Applied Catalysis a-General***375**, 1-11.
18. M. Zubair, H. Kim, A. Razzaq, C. A. Grimes, S.-I. In (2018) Solar spectrum photocatalytic conversion of CO2 to CH4 utilizing TiO2 nanotube arrays embedded with graphene quantum dots. *Journal of Co2 Utilization***26**, 70-79.
19. J. M. Herrmann (1999) Heterogeneous photocatalysis: fundamentals and applications to the removal of various types of aqueous pollutants. *Catalysis Today***53**, 115-129.
20. W. Zhou *et al.* (2010) Ag2O/TiO2 Nanobelts Heterostructure with Enhanced Ultraviolet and Visible Photocatalytic Activity. *Acs Applied Materials & Interfaces***2**, 2385-2392.
21. S. J. A. Moniz, S. A. Shevlin, D. J. Martin, Z.-X. Guo, J. Tang (2015) Visible-light driven heterojunction photocatalysts for water splitting - a critical review. *Energy & Environmental Science***8**, 731-759.
22. S. J. Hong, S. Lee, J. S. Jang, J. S. Lee (2011) Heterojunction BiVO4/WO3 electrodes for enhanced photoactivity of water oxidation. *Energy & Environmental Science***4**, 1781-1787.
23. D. Jing, L. Guo (2006) A novel method for the preparation of a highly stable and active CdS photocatalyst with a special surface nanostructure. *Journal of Physical Chemistry B***110**, 11139-11145.
24. L. Wu, J. C. Yu, X. Z. Fu (2006) Characterization and photocatalytic mechanism of nanosized CdS coupled TiO2 nanocrystals under visible light irradiation. *Journal of Molecular Catalysis a-Chemical***244**, 25-32.

25. Q. Li, X. Li, S. Wageh, A. A. Al-Ghamdi, J. Yu (2015) CdS/Graphene Nanocomposite Photocatalysts. *Advanced Energy Materials***5**.
26. L. Ge *et al.* (2012) Synthesis and Efficient Visible Light Photocatalytic Hydrogen Evolution of Polymeric g-C3N4 Coupled with CdS Quantum Dots. *Journal of Physical Chemistry C***116**, 13708-13714.
27. J. Hou *et al.* (2020) Flexible CdS and PbS nanoparticles sensitized TiO2 nanotube arrays lead to significantly enhanced photocatalytic performance. *Ceramics International***46**, 28785-28791.
28. K. Hedayati, M. Joulaei, D. Ghanbari (2020) Auto Combustion Synthesis using Grapefruit Extract: Photocatalyst and Magnetic MgFe2O4-PbS Nanocomposites. *Journal of Nanostructures***10**, 83-91.
29. X. Liu *et al.*, Fabrication of PbS quantum dots decorated ZnO nanorod arrays on Zn substrate and their visible light photocatalytic application. *Materials Letters***179**, 134-137 (2016).
30. L. Liu *et al.* (2014) Photocatalytic activity of PbS quantum dots sensitized flower-like Bi2WO6 for degradation of Rhodamine B under visible light irradiation. *Journal of Molecular Catalysis a-Chemical***394**, 309-315.
31. D. Ayodhya, G. Veerabhadram (2018) A review on recent advances in photodegradation of dyes using doped and heterojunction based semiconductor metal sulfide nanostructures for environmental protection. *Materials Today Energy***9**, 83-113.
32. T. Liu *et al.* (2018) Enhanced photoelectric performance of CdS/CdSe co-sensitized TiO2 nanosheets array films. *Sustainable Energy & Fuels***2**, 1262-1268.
33. H. Yao *et al.* (2016) Hierarchical photoanode of rutile TiO2 nanorods coupled with anatase TiO2 nanosheets array for photoelectrochemical application. *Journal of Alloys and Compounds***680**, 206-211.
34. J. C. Yu, J. G. Yu, W. K. Ho, Z. T. Jiang, L. Z. Zhang (2002) Effects of F- doping on the photocatalytic activity and microstructures of nanocrystalline TiO2 powders. *Chemistry of Materials***14**, 3808-3816.
35. J. Low, B. Dai, T. Tong, C. Jiang, J. Yu (2019) In Situ Irradiated X-Ray Photoelectron Spectroscopy Investigation on a Direct Z-Scheme TiO2/CdS Composite Film Photocatalyst. *Advanced Materials***31**.
36. J. Wu, C. Tang, H. Xu, W. Yan (2015) Enhanced photoelectrochemical performance of PbS sensitized Sb-SnO2/TiO2 nanotube arrays electrode under visible light illumination. *Journal of Alloys and Compounds***633**, 83-91.
37. Q. Zhou *et al.* (2017) Photoelectrochemical Performance of Quantum dot-Sensitized TiO2 Nanotube Arrays: , a Study of Surface Modification by Atomic Layer Deposition Coating. *Nanoscale Research Letters***12**.
38. P. V. Kamat (2012) Boosting the Efficiency of Quantum Dot Sensitized Solar Cells through Modulation of Interfacial Charge Transfer. *Accounts of Chemical Research***45**, 1906-1915.

Figures

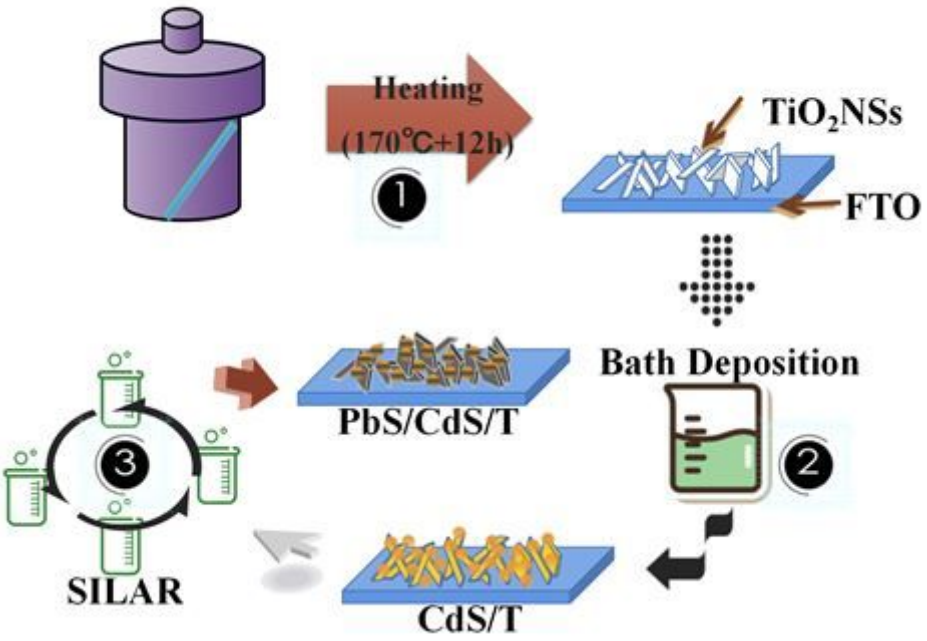

Figure 1

Illustration of the fabrication process of TiO2 NSs, CdS/TiO2 NSs and PbS/CdS/TiO2 NSs.

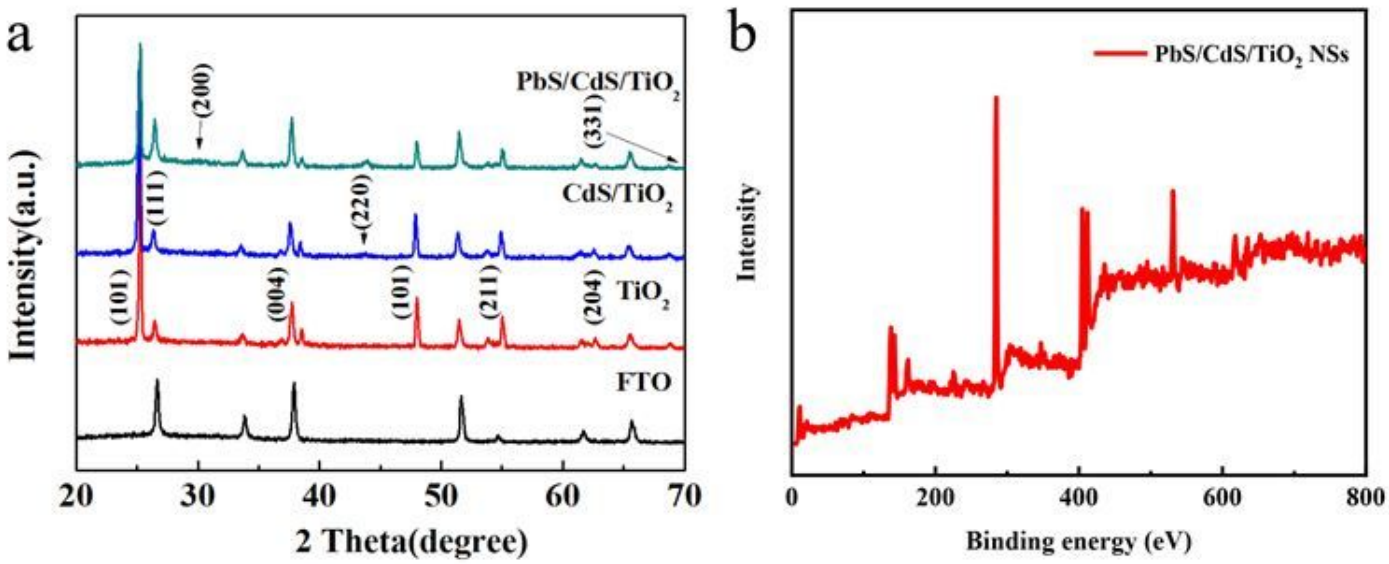

Figure 2

a) XRD patterns for TiO2, CdS/TiO2 and PbS/CdS/ TiO2.. b) XPS spectra of PbS/CdS/TiO2 NSs.

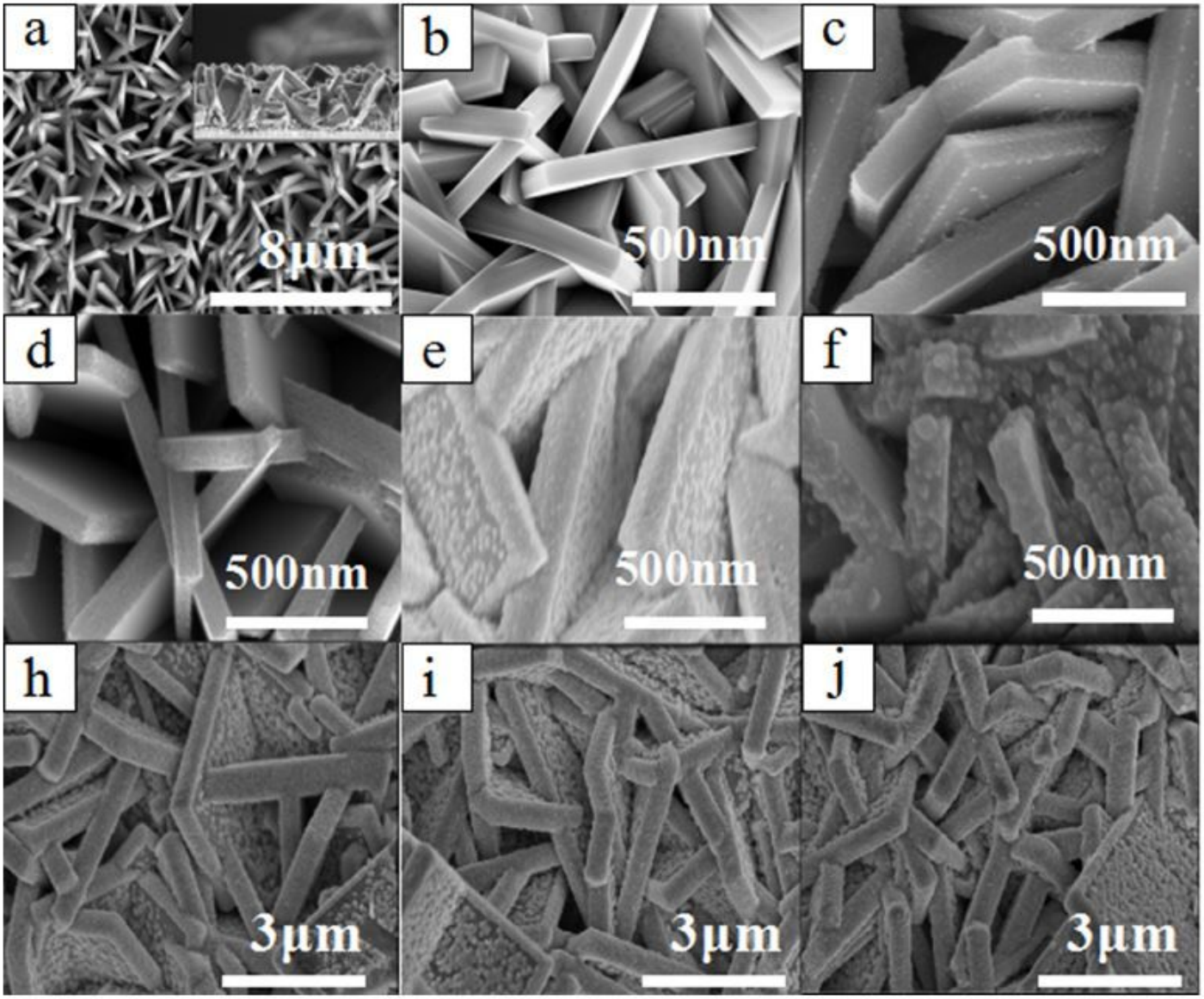

Figure 3

. a) and b) are the morphology SEM images of pristine TiO2. Inset picture is the sectional pattern of pristine TiO2. c)-f) SEM images of CdS-Sensitized TiO2 with different time(10-40min). h)-j) SEM images of PbS-Sensitized CdS/TiO2 nanocomposite with different cycles (3C, 5C, 7C).

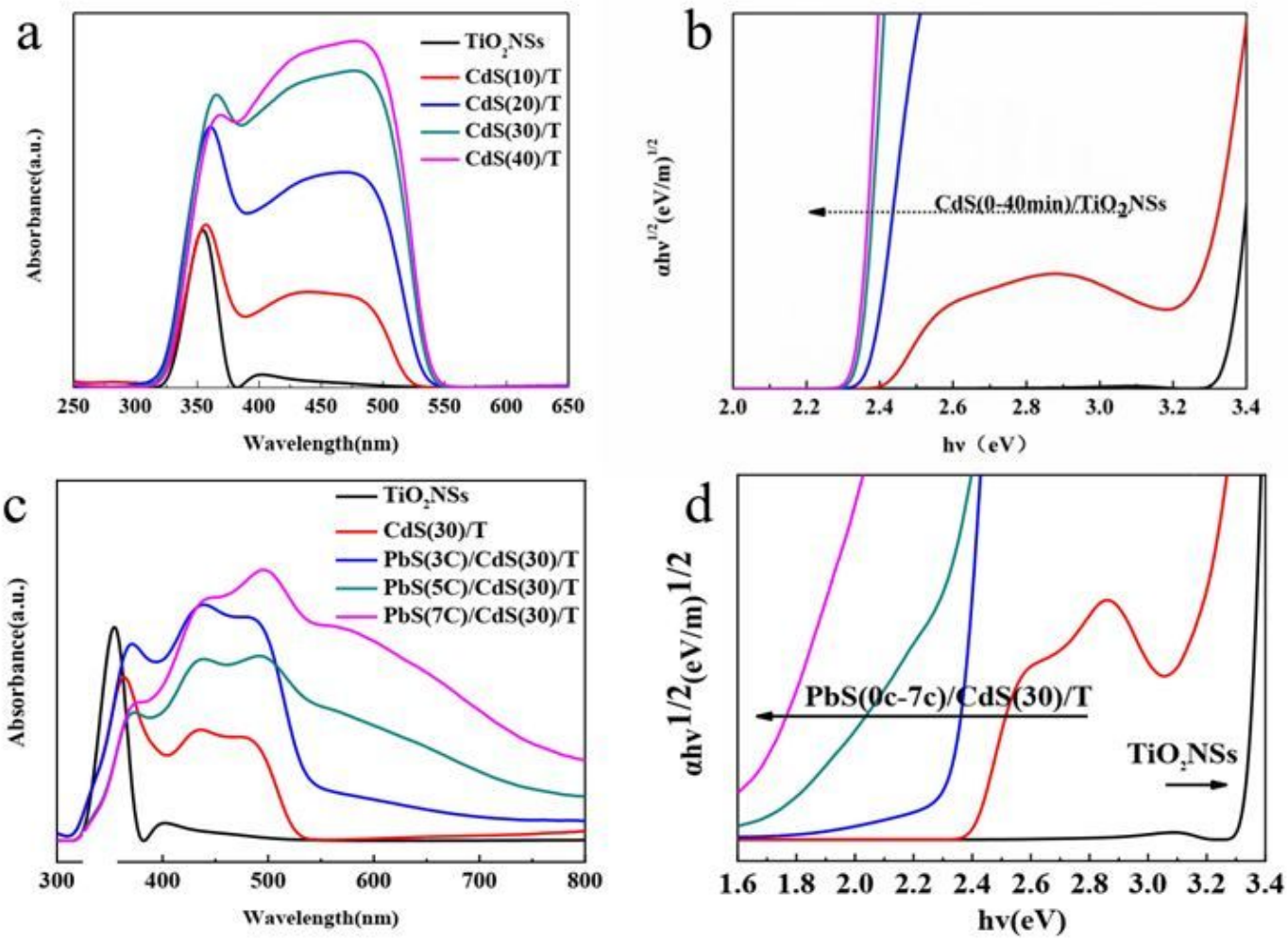

Figure 4

a) Absorption spectra and b) corresponding band gap of the pristine TiO2NSs and CdS-Sensitized TiO2 with different time(0-40min), respectively. c) Absorption spectra and d) corresponding band gap of of CdS(30)/ TiO2 and PbS-Sensitized CdS(30)/ TiO2 nanocomposite with different cycles (3C, 5C, 7C).

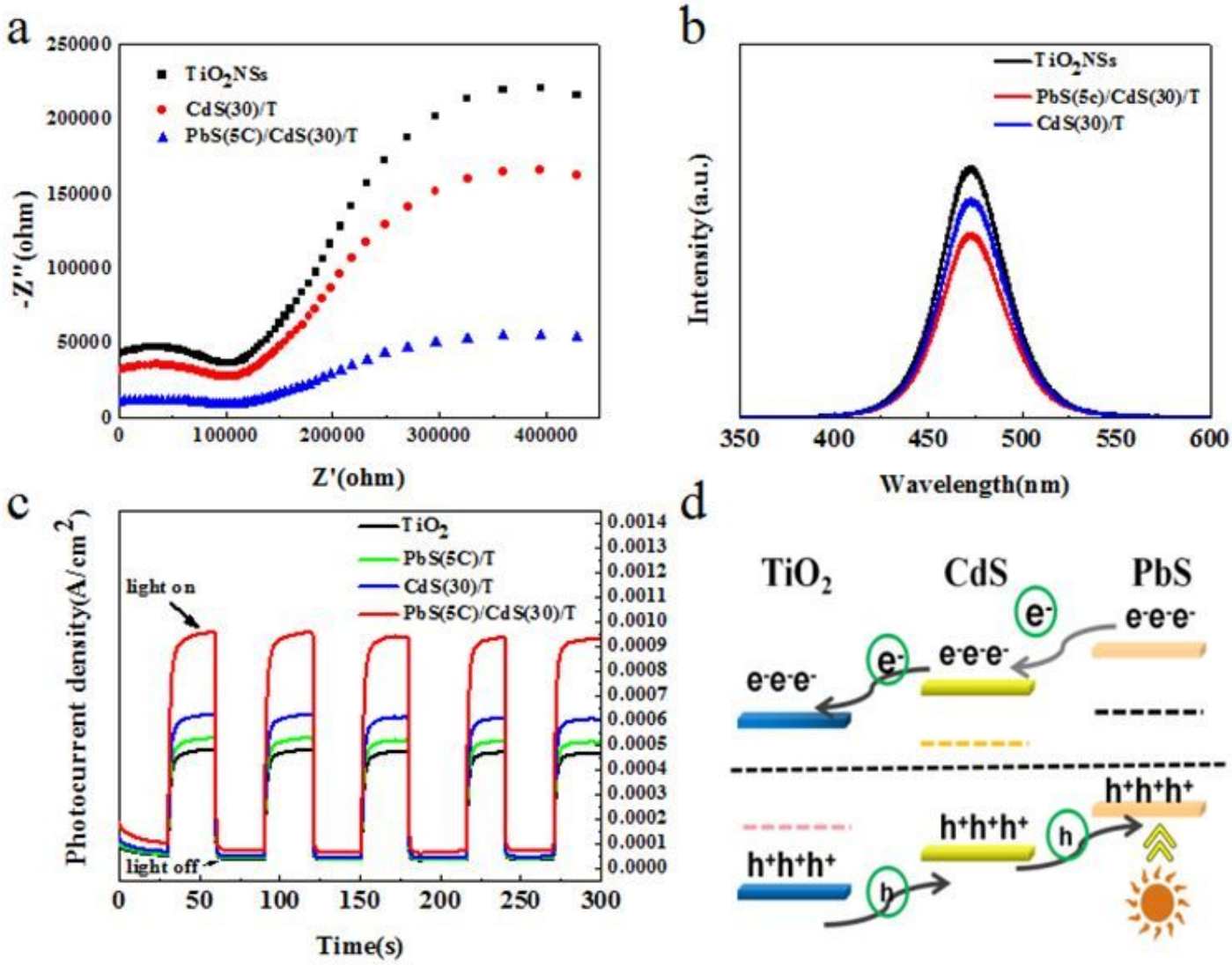

Figure 5

a) EIS Nyquist plots for optimized samples of TiO2 NSs, CdS(30)/T and PbS(5C)/CdS(30)/T, respectively. b) PL spectra of TiO2 NSs, CdS(30)/T and PbS(5C)/CdS(30)/T, respectively. c) The curves of transient photocurrent responses. d) Energy band diagram of TiO2,CdS and PbS.

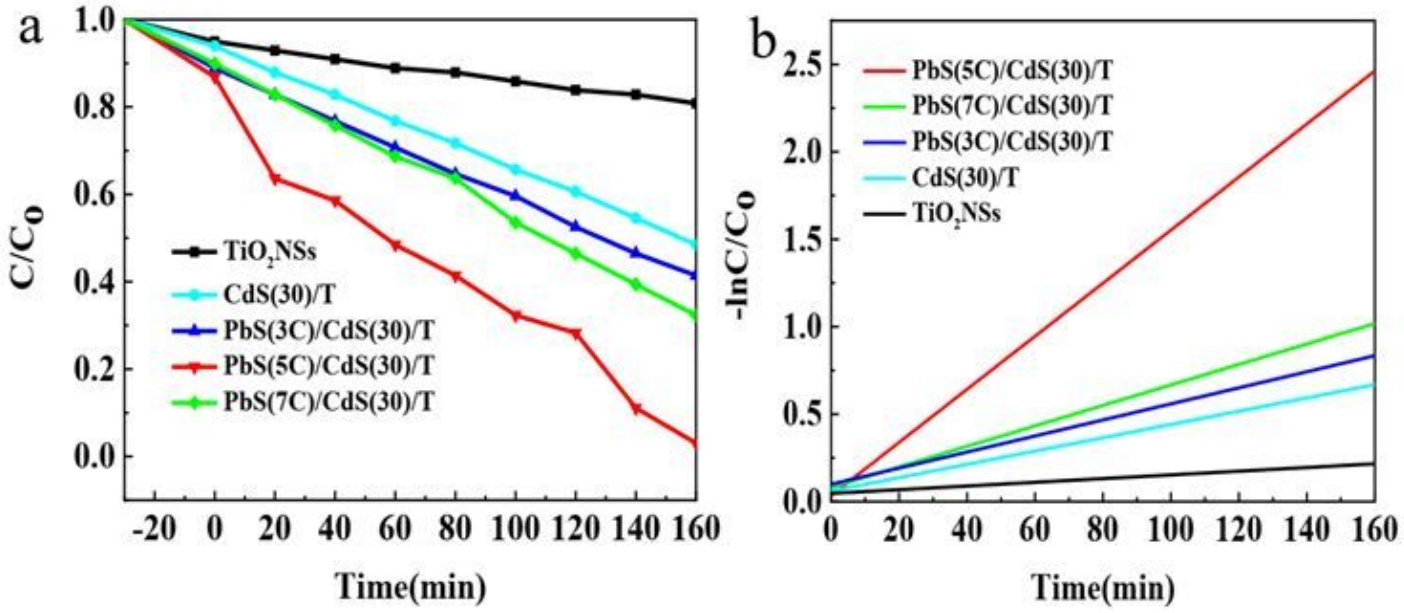

Figure 6

a) Photodegradation curves of samples under visible light irradiation (λ > 400 nm). b) The data of pseudo-first-order kinetic study of RhB degradation.

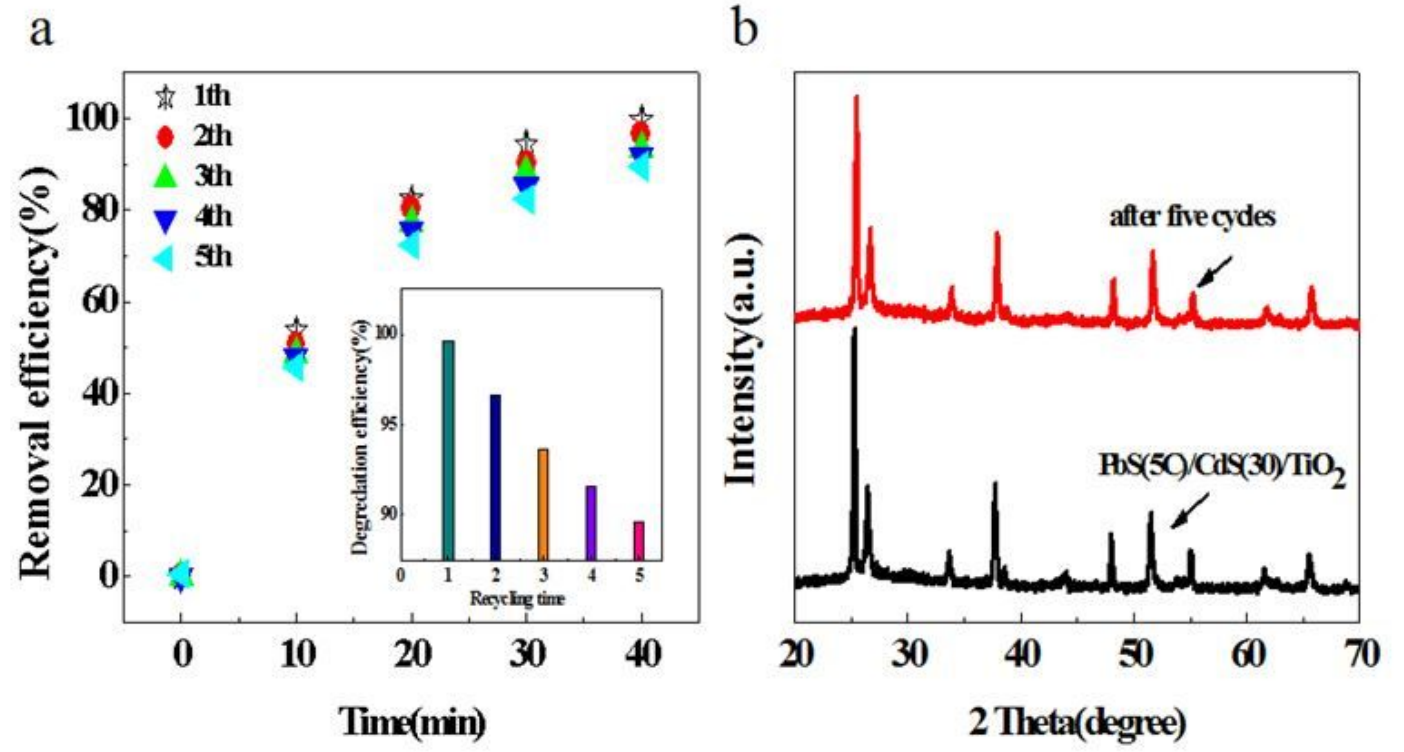

Figure 7

a) Catalyst recycling experiments for PbS/CdS/TiO2 (S=1.5cm×1.5cm) under UV light. b) XRD patterns of PbS/CdS/TiO2 NSs before and after five cycles.

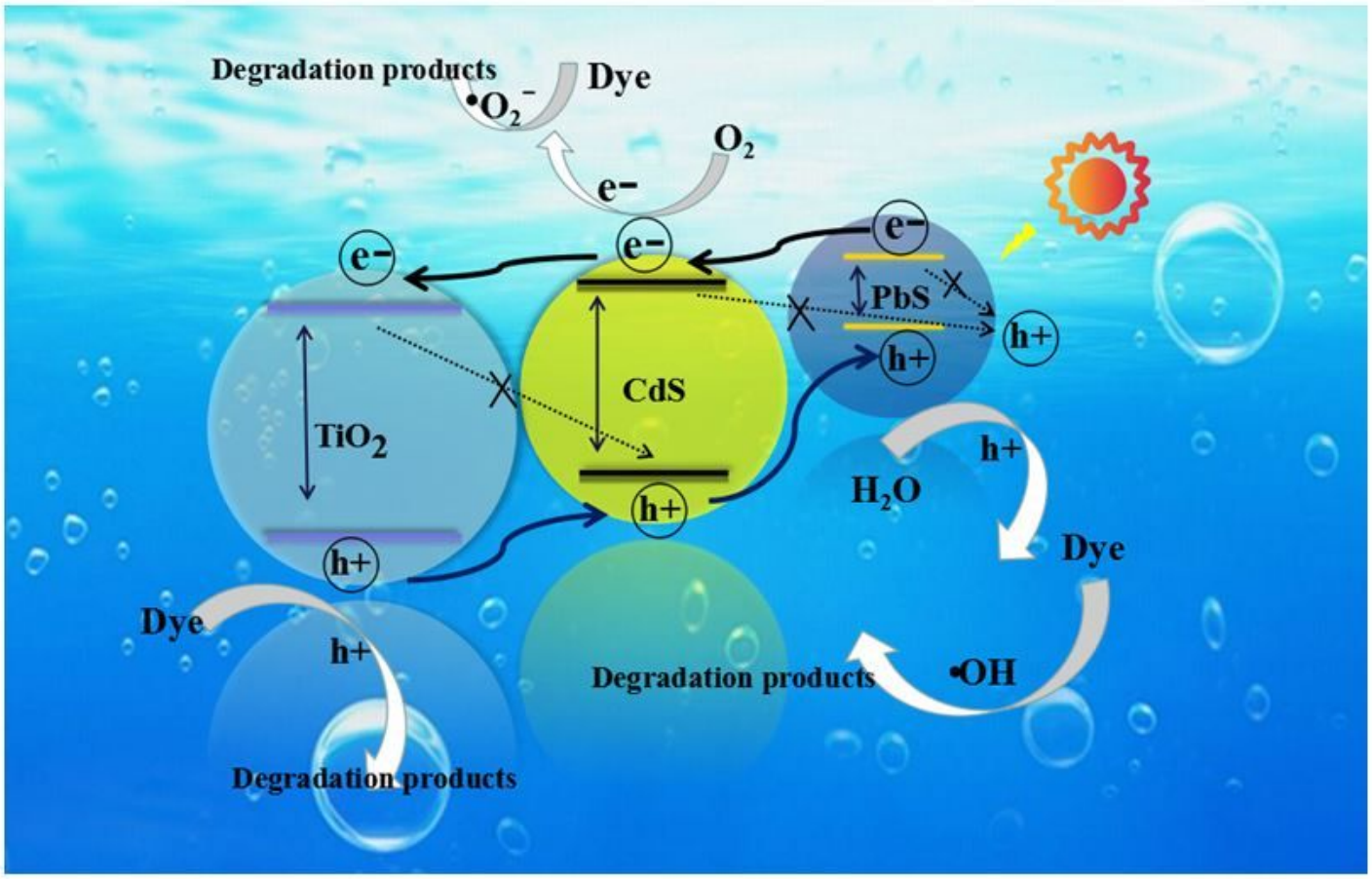

Figure 8

Schematic illustration of the proposed reaction mechanism.

Supplementary Files

This is a list of supplementary files associated with this preprint. Click to download.

- GraphicalAbstract.doc
- Highlights.doc
- Supportinginformation.doc
- formula.docx